Journal of Solid State Chemistry 187 (2012) 231–237

Contents lists available at SciVerse ScienceDirect

Journal of Solid State Chemistry

journal homepage: www.elsevier.com/locate/jssc

Structure–property correlation in epitaxial (2 0 0) rutile films on sapphire substrates

M.R. Bayati [a,*], Sh. Joshi [b], R. Molaei [a], R.J. Narayan [a,c], J. Narayan [a]

[a] Department of Materials Science and Engineering, North Carolina State University, EB-1, Raleigh 27695-7906, NC, USA
[b] Amity Institute of Nanotechnology, Noida, Uttar Pradesh-201301, India
[c] Joint Department of Biomedical Engineering, UNC Chapel Hill and North Carolina State University, EB-3, Raleigh 27695-7115, NC, USA

A R T I C L E I N F O

Article history:
Received 6 December 2011
Received in revised form
9 January 2012
Accepted 15 January 2012
Available online 24 January 2012

Keywords:
Titania
Epitaxy
Frequency
Defect
4-chlorophenol
Photocatalysis

A B S T R A C T

We have investigated the influence of the deposition variables on photocatalytic properties of epitaxial rutile films. Despite a large lattice misfit of rutile with sapphire substrate, (2 0 0) epitaxial layers were grown on (0 0 0 1)sapphire by domain matching epitaxy paradigm. Using φ-scan XRD and cross section TEM, the epitaxial relationship was determined to be rutile(1 0 0)||sapphire(0 0 0 1), rutile(0 0 1)||sapphire(1 0 −1 0), and rutile(0 1 0)||sapphire(1 −2 1 0). Based on the XRD patterns, increasing the repetition rate introduced tensile stress along the film normal direction, which may arise as a result of trapped defects. Formation of such defects was studied by UV–VIS, PL, and XPS techniques. AFM studies showed that the film roughness increases with the repetition rate. Finally, photocatalytic performance of the layers was investigated through measuring decomposition rate of 4-chlorophenol on the films surface. The films grown at higher frequencies revealed higher photocatalytic efficiency. This behavior was mainly related to formation of point defects which enhance the charge separation.
© 2012 Elsevier Inc. All rights reserved.

1. Introduction

Owing to the technologically favorable characteristics, namely large refractive index [1], high dielectric constant [2], high photochemical activity [3], high thermal [4], and photochemical stability [5], titanium dioxide (TiO_2) has been widely used in different applications in the past. Titania is known to exist primarily in three different crystal structures, i.e., rutile (tetragonal), anatase (tetragonal), and brookite (orthorhombic). The equilibrium phase is rutile which is stable at almost all temperatures. The metastable anatase phase, which is stable at low temperatures, transforms to rutile upon heating. Anatase is a low-temperature, metastable crystal and shows good photocatalytic properties [6]. It has been widely studied as a material for photocatalysis [7,8], while other properties of anatase are less known than those of rutile. Brookite exists only in some extreme conditions, so it is not considered useful for practical applications. Other structures (e.g., Magneli phases, corundum sesquioxide, and so on) also exist under extreme conditions with no practical application [9].

TiO_2 thin films have been grown by chemical vapor deposition [10], physical vapor deposition [11], sol–gel [12], micro arc oxidation [13], hydrothermal [14], and pulsed laser deposition [15] methods. Among these, pulsed laser deposition (PLD) has emerged as a promising technique for the fabrication of nanostructures of complex multicomponent materials because of its non-equilibrium characteristics and the ability to control the dimensions and the crystalline phase of nanodeposits by varying the laser parameters and the deposition conditions. This technique is also suitable for depositing oxide films at relatively low temperatures [16–18]. PLD is extensively used in the deposition of complex materials, especially multicomponent oxides [19,20], nitrides [21], polymers [22], carbides [23], etc. The quality of the films depends on various parameters like laser wavelength, energy, fluence, ambient pressure of the gas, substrate, target-substrate distance, and thermo-physical properties of the target material which include density, mass, absorption coefficient, etc. The optimization of these parameters to obtain high quality films for a desired application is, therefore, a critical part of PLD.

Even though numerous studies have focused on photocatalytic applications of anatase and anatase/rutile mixture [24–26], only few have been dedicated to the photocatalytic property of pure rutile which can be used as a visible-light-responsive material, due to its 3.0 eV band gap. Here, we focus on structure–property correlation of epitaxial rutile films grown on *c*-sapphire substrates. Previous studies did not address control of phase purity, defect, and epitaxial growth and their role on photocatalytic properties of rutile films. In this study, we deposited epitaxial

* Corresponding author. Fax: +1 919 515 7724.
E-mail address: mbayati@ncsu.edu (M.R. Bayati).

0022-4596/$ - see front matter © 2012 Elsevier Inc. All rights reserved.
doi:10.1016/j.jssc.2012.01.031

rutile TiO_2 thin films by pulsed laser deposition (PLD) technique at various repetition rates (frequencies). XRD, XPS, PL, and UV–VIS spectroscopes, and AFM methods were employed to characterize the films in terms of crystal structure and bonding properties. Photocatalytic properties of the layers were investigated through measuring degradation rate of 4-chlorophenol (4CP) as well. We show that more defective films, grown at higher repetition rates, have higher photocatalytic efficiency; whereas, films grown at lower frequencies contained less defects with reduced photocatalytic activity.

2. Experimental procedure

2.1. Films deposition

TiO_2 thin films were deposited on single crystal *c*-sapphire ($A1_20_3$) substrates by PLD method. The substrates were initially cleaned through a multi-step procedure including boiling in acetone at 150 °C for 15 min., ultrasonic cleaning in acetone for 5 min. followed by ultrasonic cleaning in methanol for 5 min. The cleaned substrates were fully dried by nitrogen gun and, then, loaded into the deposition chamber where the target–substrate distance was 4.5 cm. The chamber was evacuated to a base pressure of $\sim 1\times 10^{-6}$ Torr before injecting oxygen into the chamber to control the ambient pressure. A KrF excimer laser (λ=248 nm, τ=25 ns) was employed to ablate the TiO_2 target which was being rotated during the deposition in order to provide a uniform ablation and avoid pitting on the target surface. Laser fluence, oxygen pressure, deposition time, and substrate temperature were the same for all samples as 3.5–4.5 J cm^{-2}, 5×10^{-4} Torr, 20 min., and 450 °C, respectively. Different repetition rates of 1, 10, 20, and 30 Hz were applied in order to study effect of this parameter on properties of the layers. Immediately after deposition, the layers were thermally annealed inside the PLD chamber for 60 min. at 450 °C under oxygen pressure of 5×10^{-4} Torr.

2.2. Characterization

The crystalline structure of the TiO_2 films was investigated by $\theta-2\theta$ scanning using a Rigaku X-ray diffractometer with Cu-K_α radiation (λ=0.154 nm). The $\theta-2\theta$ scans provide out-of-plane orientation and lattice spacing for film planes parallel to the substrate. A Philips X-Pert Pro X-ray diffractometer was employed for ϕ-scanning XRD to determine in-plane orientation of TiO_2 films. In order to determine surface chemical composition and stoichiometry of the layers, X-ray photoelectron spectroscopy (XPS) was performed employing a Riber instrument with an Mg-K_α X-ray source. The samples were sputtered by Ar^+ bombardment for 5 min prior to acquiring data in order to remove any probable surface contamination. Interpretation of the XPS results was performed using SDP ver.4.1 software. Morphology of the layers was studied by a Veeco AFM as well and the obtained results were interpreted by nanoscope ver. 5.12r3 software. Optical properties of the films were studied by a U-3010 Hitachi UV–VIS spectrophotometer. The room temperature photoluminescence (PL) spectra of the samples were recorded with a fluorescence spectrophotometer (Hitachi, F-2500) where the excitation wavelength of 300 nm was used for all samples. Meanwhile, all emissions having wavelengths shorter than 420 nm were eliminated by a filter in order to highlight the peaks due to defect energy levels. The samples were masked during deposition, and their thickness was determined by a Tencor Alpha Step stylus profilometer. A JEOL-2000 FX TEM was also used to perform diffraction and imaging studies in cross section to confirm the epitaxial growth of the TiO_2 layers.

2.3. Photocatalytic studies

Photocatalytic activity of the TiO_2 layers was evaluated by measuring the degradation rate of aqueous 4-chlorophenol solution at room temperature. 50 milliliters of the 4CP solution (2×10^{-4} M) and a 1 cm × 1 cm sample, as a photocatalyst, were placed in a beaker. A medium pressure mercury lamp (λ=200–300 nm) was used as ultraviolet source during photocatalytic experiments. Prior to UV irradiation, in each experiment, the solution and the catalyst were left in the dark for 30 min (considered as a reference point) until adsorption/desorption equilibrium was reached. The solution was then irradiated by UV light. A UV–VIS spectrophotometer (Hitachi, U3010) was used to measure the change in concentration, based on the Beer–Lambert equation stating $A=\varepsilon\times b\times C$ where A, ε, b, and C are absorptance of the solution, molar absorptivity, path length, and solution concentration, respectively. Using a quartz cell, a fixed quantity of the solution was removed every 20 min to measure the absorption and, then, the concentration at a fixed wavelength of 230 nm.

3. Results and discussion

3.1. Phase structure

Fig. 1 shows XRD phase structure of the layers grown at different repetition rates where rutile(2 0 0) and sapphire(0 0 6) characteristic peaks are labeled by R and S letters, respectively. The patterns reveal that highly textured layers have been deposited. As is seen, the intensity of the rutile peak increases with the frequency. The reason for this behavior can be the deposition rate which increases with the repetition rate. As a result, thicker layers grow when higher repetition rates are applied. Thickness of the layers was measured as 418, 430, 690, and 990 nm for the repetition rates of 1, 10, 20, and 30 Hz, respectively. Meanwhile, high resolution $\theta-2\theta$ scanning was performed to determine the exact diffraction angle of the rutile(2 0 0) peak whose results are provided in the inset of Fig. 1. It is observed that the rutile peak shifts toward smaller 2θ values than the diffraction angle of the bulk rutile(2 0 0) peak (2θ=39.187°) with increasing repetition rate. This phenomenon indicates introduction of tensile stain along the direction perpendicular to the substrate surface which presumably arises from introduction of defects into the rutile

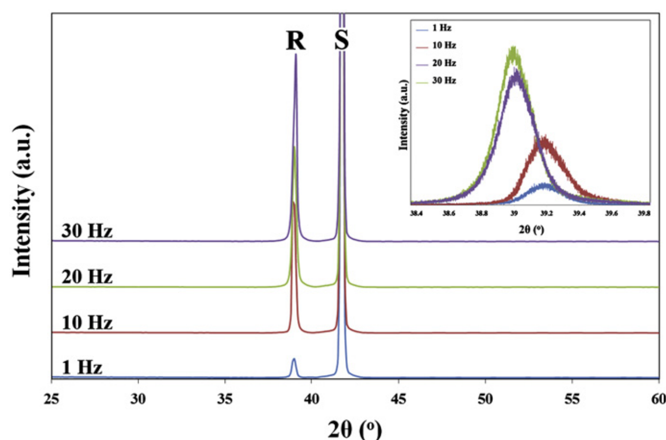

Fig. 1. Effect of the repetition rate on XRD-phase structure of the rutile films.

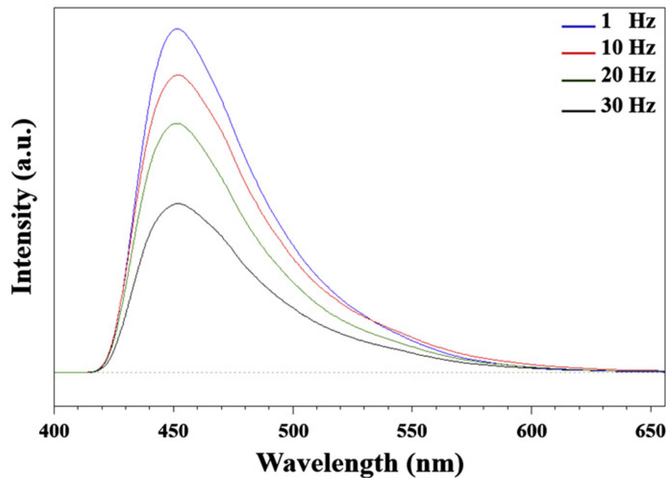

Fig. 2. Room temperature PL spectra of the rutile films grown at different frequencies.

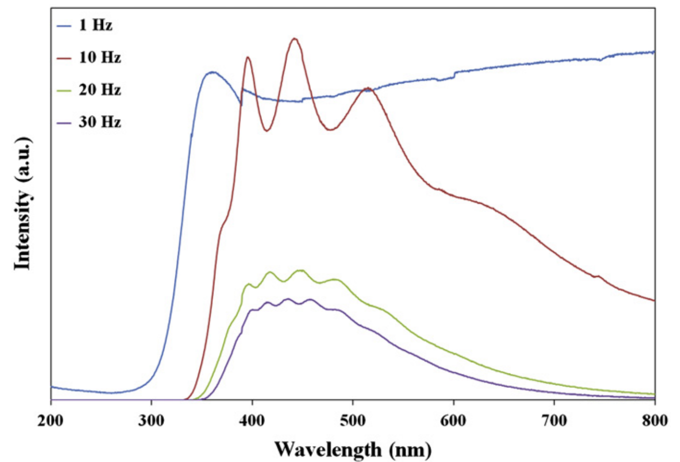

Fig. 3. Transmittance spectra of the rutile films grown at different frequencies.

crystalline lattice. At higher repetition rates, namely 30 Hz, flux of the ablated species approaching the substrate is so high and, therefore, they do not have enough time to diffuse to equilibrium positions on the substrate surface. This enhanced non-equilibrium condition gives rise to formation of a defect-rich film. Considering the XRD peak shift toward smaller diffraction angle, it may be concluded that increasing the repetition rate leads to formation of high concentration of oxygen vacancies. Full Width at Half Maximum (FWHM) of the rutile(2 0 0) peaks were determined ranging from 0.20 to 0.29 for different repetition rates.

3.2. Optical properties

Photoluminescence (PL) spectroscopy technique was also employed to study defect content in the films and the results are shown in Fig. 2. The wide emission peak located at wavelength of about 450 nm is attributed to the oxygen vacancy levels [27,28]. Any change in the PL intensities can be related to the recombination rate between the photogenerated electrons and holes [28,29]. Since the trap levels play a positive role in reducing the recombination, low PL intensity is ascribed to a lower recombination rate, and, hence, higher defect concentrations. Therefore, it is further ascertained that more oxygen vacancies form when the films are deposited at higher frequencies or repetition rates.

UV–VIS transmittance spectra of the rutile films deposited at different repetition rates are shown in Fig. 3. It was found that visible transmittance of the layers decreases with the repetition rate, which indicates creation of more structural defects at higher repetition rates. This suggestion is further confirmed by the sharper absorption edge of the layers grown at lower repetition rates, i.e., 1 and 10 Hz, which reveals less defect concentration in these films. Another reason for lower transmittance within the visible region might be the thickness of the films which increases with the repetition rate, as explained before. The oscillations in the spectra are caused by the interference light at the film/substrate interface and are attenuated when the grown films get thicker. These oscillations appear when a transparent thin film of a material having a high refractive index ($n=2.6$ for rutile) is deposited on a substrate with a lower refractive index ($n=1.7$ for sapphire).

3.3. Stoichiometry

XPS technique was employed to study stoichiometry as well as defects content of the layers and the results are shown in Fig. 4.

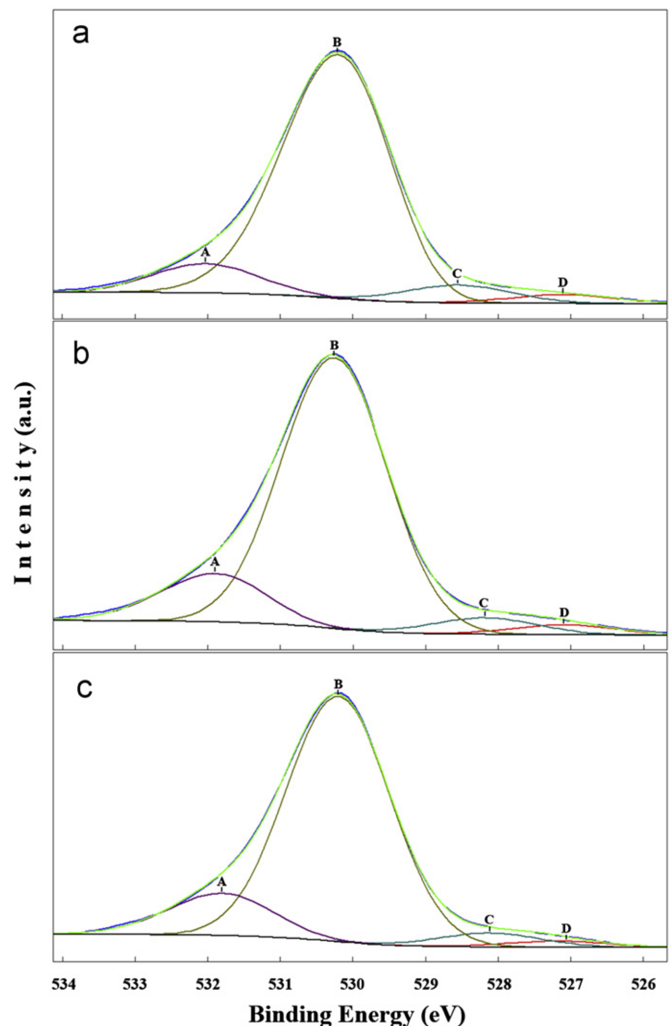

Fig. 4. O(1s) XPS core level binding energy in the rutile films grown at different frequencies: (a) 1, (b) 20, and (c) 30 Hz.

As is observed, the O(1s) core level binding energy has been fitted by 4 distinct peaks. The peak A, located at a binding energy of around 531.8 eV, corresponds to the O^{2-} ions in oxygen deficient regions and its intensity is associated with the concentration of oxygen vacancies (V_O). The peak B, having a binding energy of

530.2 eV, belongs to the oxygen ions in the crystalline lattice of perfect TiO_2. The peaks C and D, with binding energies of 528.1 and 527.2 eV, may represent oxygen atoms in contact with Ti_i^{3+} and Ti_i^{4+} defects [30]. When a titanium interstitial cation locates in rutile crystalline lattice, it attracts the electron cloud between neighboring Ti and O atoms resulting in decrease of the energy of the neighboring Ti–O bond. In conclusion, the peaks A, C, and D in O(1s) core level reflect defects content in the grown rutile films. A small peak shift is also observed for these peaks whose reason can be variation of defects concentration. Results reveal that more defects form in the crystalline lattice when higher repetition rate are applied, as discussed earlier in section 3.1.

Fig. 5. XRD ϕ-scan of the rutile(1 1 0) and sapphire (0 1 −1 2) reflection planes.

Fig. 6. TEM bright field image and indexed SAD pattern of the film/substrate interface (Rutile(0 0 1) and Sapphire(1 0 −1 0) zones, film: red, substrate: green).

Fig. 7. Schematic illustration of plausible growth mechanism of rutile TiO_2 on c-sapphire.

3.4. Epitaxial relationship

XRD ϕ-scanning was employed to confirm the epitaxial growth and determine the in-plane alignment of the (2 0 0) oriented rutileTiO_2 films on the *c*-sapphire substrate (Fig. 5). To do that, (0 1 –1 2) plane of substrate ($2\theta=25.58^\circ$, $\psi=57.70^\circ$) and (1 1 0) plane of rutile ($2\theta=27.44^\circ$, $\psi=45.00^\circ$) were selected as the reflection planes and the epitaxial relationship was established as

out-of-plane alignment: rutile(1 0 0)||sapphire(0 0 1); in-of-plane alignment: rutile(0 0 1)||sapphire(1 0 −1 0) and rutile (0 1 0)||sapphire(1 −2 1 0).

Three (0 1 −1 2) reflection intense peaks with a 120° interval originate from the threefold symmetry of the sapphire substrate. Considering six symmetrical peaks of rutile film having intervals of 60°, it is demonstrated that the film consists of three domains rotated by 120°. In other words, the orientation of the rutile film grown on the *c*-sapphire is affected by three fold symmetry of the *c*-Al_2O_3 (0 0 0 1). Fig. 6 shows TEM cross section BF-image of the rutile/sapphire sample prepared at repetition rate of 1 Hz where formation of columnar structure is evident. The columnar grain structure indicates that the threefold mosaic structure was initiated on the substrate surface via the nucleation of the three variants. The epitaxial growth as well as the proposed epitaxial relationship was confirmed by TEM-SAD pattern, depicted in the inset of Fig. 6. Indexing of this pattern shows that the diffraction spots are from the (0 0 1) zone axis of the rutile film and the (1 0 −1 0) zone axis of sapphire. Hence, it can be concluded that the rutile layer is single crystalline and grow epitaxially on *c*-sapphire substrate with the proposed orientation relationship which is schematically illustrated in Fig. 7. The rutile(1 1 0) and sapphire(0 1 –1 2) reflection planes, used for ϕ-scan XRD, are also shown in green in this figure. Lattice misfits at the film/substrate interface are calculated as follows:

$$\varepsilon_b = 1-(4.59/4.76) = +3.57\% \quad (1)$$

$$\varepsilon_c = 1-(2.96/2.86) = -3.49\% \quad (2)$$

where ε_b and ε_c are the lattice misfits along *b* and *c* directions of the film. According to the domain matching epitaxy (DME) paradigm [31], these misfits are accommodated by matching of integral multiples of lattice planes. Along the *b*-direction, 28 planes of the film match with 27 planes of the substrate with a frequency factor of $\alpha=0$ to fully relax the misfit strain. Such a frequency factor shows that there is perfect 28/27 integral multiple matching with one dislocation every 27 planes. Taking the *c*-direction into consideration, the lattice misfit was calculated as −3.49%. This misfit strain is relaxed when 28/29 and 29/30 domains alternate with a relative frequency of 6:4 (3:2). The frequency factor (α) was calculated using the following equation [31]:

$$(m+\alpha)d_f = (n+\alpha)d_s \quad (3)$$

where d_f and d_s are inter-planar spacing of film and substrate, respectively. Meanwhile, *m* and *n* are simple integers which were already calculated.

3.5. Morphology

AFM surface morphology of the rutile films is shown in Fig. 8 where formation of nanostructured films is obvious. Surface

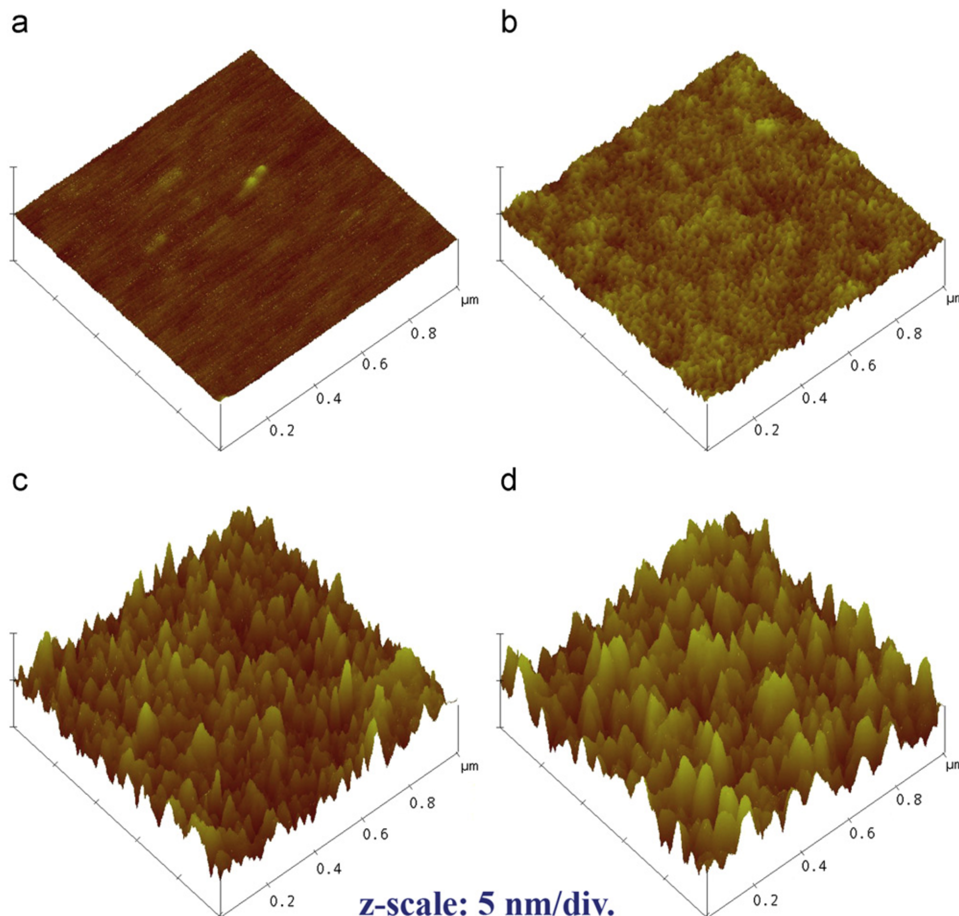

Fig. 8. AFM surface morphology of the TiO_2 films grown at frequencies of: (a) 1, (b) 10, (c) 20, (d) 30 Hz.

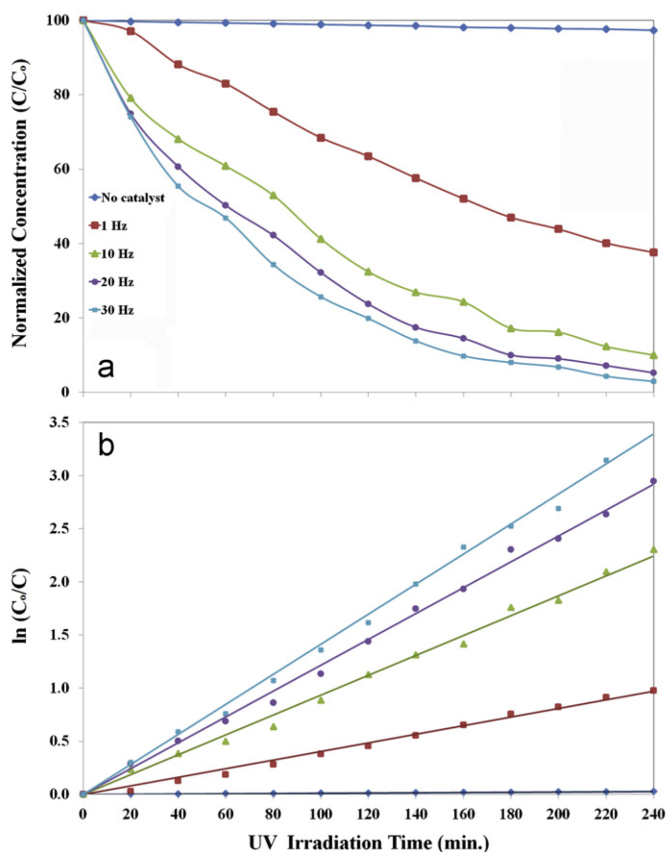

Fig. 9. Photocatalytic activity of the rutile TiO_2 thin films: (a) normalized concentration of 4CP and (b) $ln(C_o/C)$ at different UV-irradiation times.

roughness of the layers was determined as 0.9, 2.1, 7.3, and 8.5 nm for repetition rates of 1, 10, 20, and 30 Hz. At low frequencies, the deposition rate is low and the ablated species have enough time to diffuse onto the substrate surface and find appropriate surface positions and create a smooth surface. In contrast, when high frequencies, i.e., 20 and 30 Hz, are applied, the adatoms do not have enough time to locate on proper surface sites with the lowest free energy.

3.6. Photocatalytic performance

Results of photocatalytic experiments are shown in Fig. 9. Results show that concentration of 4CP decreases with illumination time; that is, 4CP is photocatalytically decomposed by the UV-activated TiO_2 films. It should be noted that the curve "No catalyst" belongs to the experiment where no sample was used as catalyst and only the 4CP solution was irradiated by the UV light. This experiment was considered as the reference point. In order to quantitatively compare the photocatalytic activity of the layers, the photocatalytic reaction rate constants (k) should have been calculated. Since photocatalytic decomposition of 4CP solution agrees with pseudo-first-order kinetics, the constant (k) can be calculated by the equation $ln(C/C_o)=-kt$ (where C_o is the initial concentration of 4CP at $t=0$ and C represents the concentration of 4CP at later times t). The quantity $ln(C_o/C)$ versus irradiation time was plotted for different repetition rates. Straight lines, whose slopes represent k, indicate that the degradation of 4CP is a first order reaction. The reactions rate values (listed in Table 1) show that the photocatalytic activity increases with repetition rate. Two reasons can be proposed for this behavior. First, effective surface area of the grown catalysts, where photocatalytic reactions take place, increases at higher repetition rates, as is seen in

Table 1
Photocatalytic reaction rate constants (k) as a function of the frequency.

Frequency (Hz)	1	10	20	30
k ($_{min.}{}^{-1}$)	0.00431	0.00952	0.01210	0.01440

k for "no catalyst" experiment = 0.000109 min.$^{-1}$.

Fig. 9. Second, it was already shown that films with higher defect content grow when higher repetition rates are applied. The structural defects, namely V_O, trap photogenerated electrons and, consequently, enhance charge separation so that positive holes which are prerequisite for photocatalytic decomposition of 4CP can participate in reactions without recombination. According to the literature [32] and our results, following reactions are put forward for photocatalytic degradation of 4CP over defected rutile TiO_2 catalyst:

$$TiO_2 + h\upsilon \rightarrow e^- + h^+ \quad (4)$$

$$e^- + V_O \rightarrow \text{trapped electrons} \quad (5)$$

$$h^+ + H_2O \rightarrow H^+ + OH \quad (6)$$

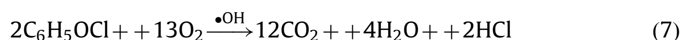

$$2C_6H_5OCl + +13O_2 \xrightarrow{\bullet OH} 12CO_2 + +4H_2O + +2HCl \quad (7)$$

Since TiO_2 films are (2 0 0) epitaxial surface, the observed photocatalytic activity is attributed to (2 0 0) surface, morphology, and defect.

4. Concluding remarks

The rutile epitaxial layers with a (2 0 0) orientation were grown on c-cut sapphire substrate employing PLD technique where an epitaxial relationship as rutile(1 0 0)(0 1 0)|| sapphire(0 0 1)(1 −2 1 0) was proposed. The rutile (2 0 0) characteristic peak was observed to shift toward smaller 2θ values when repetition rate increased. The reason for such a behavior was assumed to be developing a tensile stress along out-of-plane direction due to formation of oxygen vacancies. The films grown at higher repetition rates revealed a rougher surface which was suitable for photocatalytic application. The rutile films grown at higher repetition rates exhibited higher photocatalytic efficiency and could decompose about 97% of 4CP after 240 min. UV-irradiation.

Acknowledgment

Financial support of the U.S.A. National Science Foundation (NSF) is highly appreciated.

References

[1] Y. Yamada, H. Uyama, T. Murata, H. Nozoye, Vacuum 66 (2002) 347–352.
[2] G. Liu, W. Jian, H. Jin, Z. Shi, G. Qiao, Script. Mater. 65 (2011) 588–591.
[3] F. Dong, H. Wang, Z. Wu, J. Qiu, J. Colloid Interface Sci. 343 (2010) 200–208.
[4] Y. Li, X. Sun, H. Li, S. Wang, Y. Wei, Powder Technol. 194 (2009) 149–152.
[5] D. Li, H. Huang, X. Chen, Z. Chen, W. Li, D. Ye, X. Fu, J. Solid State Chem. 180 (2007) 2630–2634.
[6] A. Fujishim, X. Zhang, D.A. Tryk, Surf. Sci. Rep. 63 (2008) 515–582.
[7] F.G. Gassim, A.N. Alkhateeb, F.H. Hussein, Desalin 209 (2007) 342–349.
[8] L.H. Kao, T.C. Hsu, K.K. Cheng, J. Colloid Interface Sci. 341 (2010) 359–365.
[9] R. Roy, W.B. White, J. Cryst. Growth 14/14 (1972) 78–83.
[10] H. Xie, L. Zhu, L. Wang, S. Chen, D. Yang, L. Yang, G. Gao, H. Yuan, Particuology 9 (2011) 75–79.
[11] P. Singh, D. Kaur, Physica B 405 (2010) 1258–1266.
[12] N. Zhao, M. Yao, F. Li, F. Lou, J. Solid State Chem. 10.1016/j.jssc.2011.08.014.
[13] M.R. Bayati, A.Z. Moshfegh, F. Golestani-Fard, Electrochim. Acta 55 (2010) 3093–3102.

[14] Y. Huang, G. Xie, S. Chen, S. Gao, J. Solid Sate Chem. 184 (2011) 502–508.
[15] G. Socol, Y. Gnatyuk, N. Stefan, N. Smirnova, V. Djokić, C. Sutan, V. Malinovschi, A. Stanculescu, O. Korduban, I.N. Mihailescu, Thin Solid Films 518 (2010) 4648–4653.
[16] D.B. Chrisey, G.K. Huber (Eds.), Pulsed Laser Deposition of Thin Films, Wiley, New York, 1994.
[17] R.K. Singh, J. Narayan, Phys. Rev. B 41 (1990) 8843–8859.
[18] R. Eason (Ed.), Pulsed Laser Deposition of Thin Films: Applications-led Growth of Functional Materials, Wiley, New York, 2006.
[19] W. Wei, S. Nori, C. Jin, J. Narayan, R.J. Narayan, D. Ponarin, A. Smirnov, Mater. Sci. Eng. B 171 (2010) 90–92.
[20] S. Mal, T.H. Yang, P. Gupta, J.T. Prater, J. Narayan, Acta Mater. 59 (2011) 2526–2534.
[21] F. Tian, E.F. Chor, Thin Solid Films 518 (2010) e121–e124.
[22] R. Cristescu, C. Popescu, A. Popescu, S. Grigorescu, I.N. Mihailescu, D. Mihaiescu, S.D. Gittard, R.J. Narayan, T. Buruiana, I. Stamatin, D.B. Chrisey, Appl. Surf. Sci. 255 (2009) 9873–9876.
[23] R. Teghil, A. De Bonis, A. Galasso, P. Villani, A. Santagata, D. Ferro, S.M. Barinov, Appl. Surf. Sci. 255 (2009) 5220–5223.
[24] M.R. Bayati, F. Golestani-Fard, A.Z. Moshfegh, Mater. Chem. Phys. 120 (2010) 582–589.
[25] M.R. Bayati, F. Golestani-Fard, A.Z. Moshfegh, R. Molaei, Mater. Chem. Phys. 128 (2011) 427–432.
[26] M.R. Bayati, R. Molaei, A. Kajbafvala, S. Zanganeh, H.R. Zargar, K. Janghorban, Electrochim. Acta 55 (2010) 5786–5792.
[27] Q. Xiao, L. Ouyang, L. Gao, W. Jiang, Mater. Chem. Phys. 124 (2010) 1210–1215.
[28] Y. Cong, J. Zhang, F. Chen, M. Anpo, J. Phys. Chem. C. 111 (2007) 6976–6982.
[29] K.V. Baiju, A. Zachariah, S. Shukla, S. Biju, M.L.P. Reddy, K.G.K. Warrier, Catal. Lett. 130 (2009) 130–136.
[30] B. Liu, X. Zhao, Q. Zhao, X. He, J. Feng, J. Electron. Spectrosc. Relat. Phenom. 148 (2005) 158–163.
[31] J. Narayan, B.C. Larson, J. Appl. Phys. 93 (2003) 278–285.
[32] Y. Cheng, H. Sun, W. Jin, N. Xu, Chem. Eng. J. 128 (2007) 127–133.